RESEARCH ARTICLE | SEPTEMBER 09 2024

Characteristic investigation of digital control four quadrant electro-hydrostatic actuator with separated hydraulic motor

Xiaoming Chen ; Yuchuan Zhu ; Jie Ling ; Mingming Zhang

Rev. Sci. Instrum. 95, 095002 (2024)
https://doi.org/10.1063/5.0214168

Review of Scientific Instruments ARTICLE pubs.aip.org/aip/rsi

Characteristic investigation of digital control four quadrant electro-hydrostatic actuator with separated hydraulic motor

Cite as: Rev. Sci. Instrum. 95, 095002 (2024); doi: 10.1063/5.0214168
Submitted: 16 April 2024 • Accepted: 15 August 2024 •
Published Online: 9 September 2024

Xiaoming Chen,[1,2] Yuchuan Zhu,[1,a)] Jie Ling,[1] and Mingming Zhang[1]

AFFILIATIONS

[1] College of Mechanical and Electrical Engineering, Nanjing University of Aeronautics and Astronautics, Nanjing 210016, China
[2] The First Aircraft Institute, AVIC, Xi'an 710089, China

[a)] **Author to whom correspondence should be addressed:** meeyczhu@nuaa.edu.cn

ABSTRACT

The asymmetric electro-hydrostatic actuator (EHA) is a promising distributed hydraulic actuation solution for the more-electric aircraft (MEA). However, the flow asymmetry is a common problem causing the poor position control accuracy and dynamics of EHA. To achieve good flow control in all quadrants and save energy in the assistive quadrants, a digital control four quadrant electro-hydrostatic actuator with a separated hydraulic motor using a novel four-quadrant division principle was proposed in this article. The theoretical model of the proposed EHA has been developed in MATLAB/Simulink and validated in the experiments. The theoretical results indicated that the increased external force allows the proposed EHA to have a constantly and partly linearly and varied motion velocity of the cylinder piston in the resistive and assistive quadrants, and the latter is determined by the specific external forces of 0.5 and 2.8 kN, respectively, in the extension and retraction quadrants. Compared with EHA without SHM, in the second and fourth quadrants, the energy dissipation is reduced by 104% and 36.7%, respectively, while the motion velocity of the cylinder piston is reduced by 12.9% and 25.6%, respectively. The theoretical and experimental results indicated that the proposed four quadrants division method effectively corrects the misjudgment of quadrants by using the existing four quadrants division method under the lower external force.

I. INTRODUCTION

As a compactness solution to aircraft actuation, the electro-hydrostatic actuator (EHA) is a pump-controlled drive system typically, which has the advantage of being energy-saving compared to a valve-controlled actuator.[1] EHA is usually integrated by an electric servo motor, a dual-directional hydraulic pump, functional hydraulic valves, a hydraulic cylinder, and a supercharged tank or an accumulator.[2] In comparison with the conventional lumped hydraulic actuation system applied in flight control systems, the distributed EHA is independent of the number of pipelines to transfer power but relies on the power by wire (PBW),[3] employing the advantages of high energy-efficiency, high reliability, and low maintenance.[4] Recent research also demonstrates that the efficiency of the EHA is better than that of the lumped hydraulic actuation system, except for dynamics.[5] Meanwhile, EHA works as a significant component in the development of more-electric or even all-electric aircraft.[6] The characteristics exploration of EHA is essential to the flight control system performance of the aircraft, especially fighters that require high maneuverability.[7]

To adapt the complex requirements of a flight control system, several EHA architectures were proposed, such as a variable rotation speed control scheme implemented[1] by a fixed displacement pump and variable speed electric servo motor (FPVM),[8] a variable displacement control scheme executed by a variable displacement pump and fixed speed electric servo motor (VPFM),[9] and a simultaneous variable displacement and rotation speed control scheme realized by a variable displacement pump and variable speed electric servo motor (VPVM).[10] The fact that the majority of applications are based on the FPVM-EHA with an asymmetric cylinder,[11] which is a promising alternative to the conventional electro-hydraulic servo system due to its compactness, large output force, and efficiency.[12]

However, the flow asymmetry caused by differential cylinder areas limits its performance and application.[13]

To address the flow asymmetry, several solutions were explored, such as utilizing individual pumps connected to each cylinder port,[14] pumps with multiple flow ports,[15] hydraulic transformers,[16] and directional or flow control valves.[17] The pump-compensation solutions cause higher costs and more complex structures, reducing the EHA's compactness[18] in comparison with flow allocation strategies modulated by functional valves such as a pilot operated check valve[19] and an internal pilot operated closed center shuttle valve.[20] Due to the intrinsic pilot ratio and pressure-dependent dynamics,[21] these passive dependent hydraulic pilot operated valves fail to maintain a certain dynamics under varying load conditions. The digital on–off valve is a promising substitute for these common flow control valves undoubtedly, due to its advantages of low cost, fast response, and low sensitivity contamination.[22] The bypass layout of digital on–off valves can be realized for flow compensation or recuperation in all conditions for an EHA.[23]

In practical terms, an EHA in the flight control systems requires different motions for a variety of load conditions.[24] The required motions can be typically classified into the four quadrant modes, including resistive extension, assistive extension, resistive retraction, and assistive retraction.[25] In the resistive extension or retraction, the electric servo motor acts as a drive and consumes the electric energy. When the EHA works in the assistive extension or retraction, the electric servo motor acts as a brake, causing a severe burden for power supply.[26] Besides, the EHA integrated installation results in a small heat dissipation area, leading to excessive throttling loss that evolves into temperature rise in the assistive quadrants.[27] Meanwhile, the elimination of a centralized oil source in EHAs restricts the cooling capacity of the system, leading to potential adverse effects on performance and longevity caused by excessively elevated temperatures.[28] To solve these issues, some researchers proposed the motor–pump assembly[29] and the bypass hydraulic circuits characterized by the flow control valve and accumulator to recycle the hydraulic energy timely.[30] Due to the intrinsic architecture of rotational speed and displacement, the ability of motor–pump assembly on flow and energy fails to acquire better performance under a wide range of working conditions.[29] Besides, the flow capacities of bypass flow control valves are pre-matched usually; the large load enables it to experience extra power dissipation, causing the limited motion velocity in the assistive quadrants; even digital on–off valves are no exception.[23]

Recent research achievement indicated that energy savings exceeding 75% derived from energy regeneration and minimal throttling loss can be acquired through the designed bypass hydraulic circuit architecture for an EHA, leading to EHA enabling efficient and reliable assistive and resistive operation.[31] Hence, either the differentiated flow allocation or energy exchange above-mentioned is dependent on the four quadrant division.[32] Costa and Sepehri[33] found that the previous quadrant division results in either geometric quadrants that do not coincide with motoring and pumping operations or misrepresentations of the actual energy exchange between the load and cylinder. Qu *et al.*[34] also thought the current definition of four quadrants makes it difficult to describe the transition of energy exchange and flow demand in the motoring and pumping mode. A novel definition of quadrants is given, and the operation of compensating flow valves can be correctly presented.[33] The implementation of the four quadrant mode is based on an integrated pump/motor,[35] which also probably harms the driver of the electric servo motor.[30] The separated hydraulic motor circuit can avoid the issue and performs as an effective way to flow allocation efficiently.[36] The combination of a digital on–off valve and a separated hydraulic motor circuit makes the division of EHA into four quadrant operational modes apparent.[37,38] To address the flow asymmetry and achieve high energy efficiency, a digital control four-quadrant electro-hydrostatic actuator with a separated hydraulic motor and corrected four-quadrant division methodology were proposed in this article.

This article is organized as follows: Sec. II presents the configuration and operational quadrants of the proposed EHA. The theoretical models of the proposed EHA are developed in Sec. III. Section IV discusses the EHA performance theoretically, and the experimental validations are presented in Sec. V, followed by the conclusions in Sec. VI.

II. CONFIGURATION AND PRINCIPLE OF EHA

A. Configuration of EHA

The proposed EHA (as shown in Fig. 1) mainly consists of an electric servo motor (MOT), a fixed displacement gear pump (DFP), a separated hydraulic motor (SHM), an accumulator (ACC), a 2/3 way digital on–off valve (FSV03), two manual relief valves (RV01, RV02), two 2/2 way digital on–off valves (FSV01, FSV02), two cartridge check valves (CV01, CV02), and an asymmetric hydraulic cylinder (AHC).

The electric servo motor is capable of adjusting the discharge flow rate of the hydraulic pump to satisfy the flow demands of EHA motion. The main purpose of relief valves is to constrain the generated pressure difference between the piston-side cylinder chamber and the rod-side cylinder chamber. The 2/2 way digital on–off valve located in the bypass hydraulic circuit is used to implement the flow compensation or recuperation at the different occasions. The check valves incorporated into the external leakage drain of the hydraulic pump are used to replenish oil. The role of a 2/3 way valve

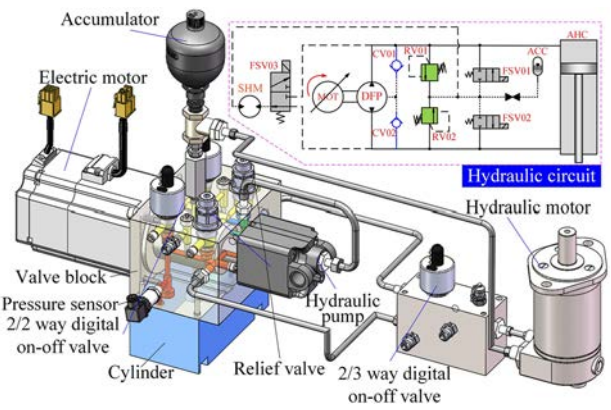

FIG. 1. Hydraulic circuit and schematic of proposed EHA.

connects the piston-side or rod-side cylinder chambers to the separated hydraulic motor alternatively according to the demands. The accumulator aims at eliminating the flow differential between the piston-side and rod-side cylinder chambers.

B. Operational quadrants of EHA

The four operational quadrants (as demonstrated in Fig. 2) are divided into resistive extension (first quadrant), assistive extension (second quadrant), resistive retraction (third quadrant), and assistive retraction (fourth quadrant). The motion velocity of the cylinder piston is represented by the abscissa. The external forces exerted on the cylinder piston are divided into inward and outward forces, and the net force is represented by the ordinate.

In the first quadrant, the piston-side cylinder chamber is pressurized by pump discharge flow, and the cylinder piston extends against the inward external force. In the second quadrant, the rod-side cylinder chamber is passively pressurized by the outward external force, and the cylinder piston is forced to extend. In the third quadrant, the rod-side cylinder chamber is pressurized by reverse pump discharge flow and the cylinder piston retracts against the outward external force. In the fourth quadrant, the piston-side is pressurized by the inward external force passively, and the cylinder piston is forced to retract. According to the first law of thermodynamics, the energy equilibrium that occurred at the actuator in the four operational quadrants can be successively represented by the equations as

$$\left(m_{\mathrm{p}}\frac{\mathrm{d}v_{\mathrm{p}}}{\mathrm{d}t}+F_{\mathrm{e}}+F_{\mathrm{cf}}\right)v_{\mathrm{p}}=(p_{\mathrm{p}}-\alpha p_{\mathrm{a}})A_{\mathrm{p}}v_{\mathrm{p}}, \tag{1}$$

$$\left(m_{\mathrm{p}}\frac{\mathrm{d}v_{\mathrm{p}}}{\mathrm{d}t}+F_{\mathrm{e}}-F_{\mathrm{cf}}\right)v_{\mathrm{p}}=(\alpha p_{\mathrm{a}}-p_{\mathrm{p}})A_{\mathrm{p}}v_{\mathrm{p}}, \tag{2}$$

$$\left(m_{\mathrm{p}}\frac{\mathrm{d}v_{\mathrm{p}}}{\mathrm{d}t}+F_{\mathrm{e}}+F_{\mathrm{cf}}\right)v_{\mathrm{p}}=(\alpha p_{\mathrm{a}}-p_{\mathrm{p}})A_{\mathrm{p}}v_{\mathrm{p}}, \tag{3}$$

$$\left(m_{\mathrm{p}}\frac{\mathrm{d}v_{\mathrm{p}}}{\mathrm{d}t}+F_{\mathrm{e}}-F_{\mathrm{cf}}\right)v_{\mathrm{p}}=(p_{\mathrm{p}}-\alpha p_{\mathrm{a}})A_{\mathrm{p}}v_{\mathrm{p}}, \tag{4}$$

where m_{p} is the mass of the cylinder piston, v_{p} is the motion velocity of the cylinder piston, A_{p} is the area of the piston-side cylinder chamber, α is the area ratio of the rod-side cylinder chamber and piston-side cylinder chamber, F_{e} is the external force, and F_{cf} is the friction force, which is always opposite to the motion velocity of the cylinder piston. Here, different from the common force equilibrium equation, the damping forces that should have appeared in Eqs. (1)–(4) are neglected due to having a little influence on either the resultant force or the quadrant division.[33]

To simplify the four quadrant division, judging the located quadrant according to the positive and negative of the right term shown in Eqs. (1)–(4) in this article. The specific method is as follows: $(p_{\mathrm{p}}\text{-}\alpha p_{\mathrm{a}})A_{\mathrm{p}}v_{\mathrm{p}} > 0$ represents the resistive quadrants, and $(p_{\mathrm{p}}\text{-}\alpha p_{\mathrm{a}})A_{\mathrm{p}} > 0 \& v_{\mathrm{p}} > 0$ represents the first quadrant, as well as $(p_{\mathrm{p}}\text{-}\alpha p_{\mathrm{a}})A_{\mathrm{p}} < 0 \& v_{\mathrm{p}} < 0$ represents the third quadrant. $(p_{\mathrm{p}}\text{-}\alpha p_{\mathrm{a}})A_{\mathrm{p}}v_{\mathrm{p}} < 0$ represents the assistive quadrants, and $(p_{\mathrm{p}}\text{-}\alpha p_{\mathrm{a}})A_{\mathrm{p}} < 0 \& v_{\mathrm{p}} > 0$ represents the second quadrant, as well as $(p_{\mathrm{p}}\text{-}\alpha p_{\mathrm{a}})A_{\mathrm{p}} > 0 \& v_{\mathrm{p}} < 0$ represents the fourth quadrant.

III. THEROETICAL MODEL OF EHA

The asymmetric electro-hydrostatic actuator is usually considered to be a complex system, and its performance significantly affects the characteristics of the main functional modules, including the main supply flow circuit, bypass digital flow circuit, and actuation circuit. The main supply flow circuit is implemented by a fixed displacement hydraulic pump driven by an electric servo motor. The bypass digital flow circuit is dependent on an accumulator, two 2/2 way digital on–off valves, and two check valves. The actuation circuit is represented by the dynamics of the cylinder piston and separated hydraulic motor.

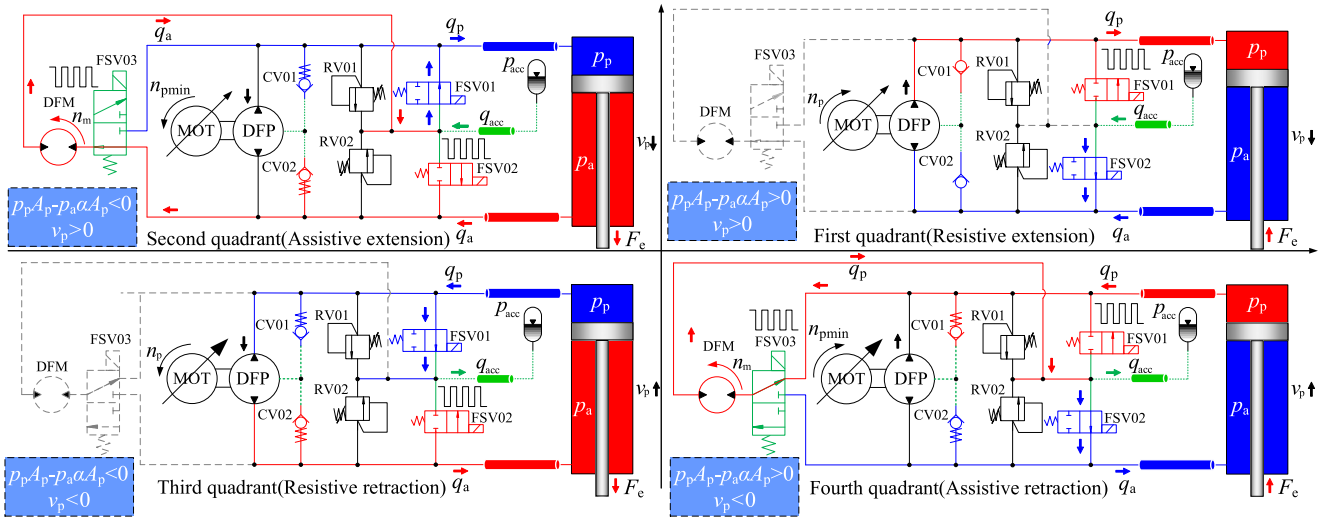

FIG. 2. Four operational quadrants of proposed EHA.

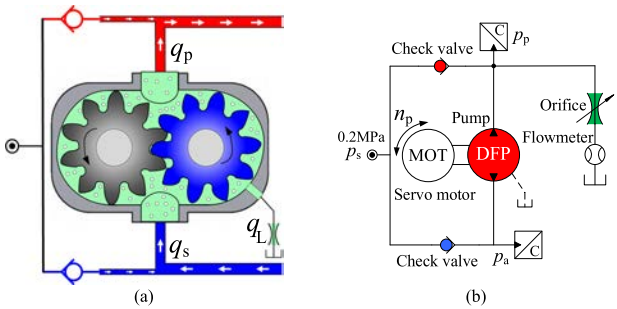

FIG. 3. (a) Schematic diagram of the pump. (b) Test the hydraulic circuit.

A. Main supply flow circuit

The hydraulic pump converts the mechanical energy provided by the electric servo motor to generate fluid flow and static pressure distribution. A bidirectional fixed displacement hydraulic gear pump employs four ports, including a discharge port p_p, a suction port p_a, a supply port p_s, and an external leakage drain q_L, as demonstrated in Fig. 3.

The supply port p_s provides suction flow rate for the pump due to the clockwise or anti-clockwise rotation of the electric servo motor. The external leakage drain is recuperated as an auxiliary flow source. The discharge port p_p and suction port p_a are initially connected to the piston-side and rod-side cylinder chambers of the asymmetric hydraulic cylinder, respectively. The discharge port and suction port can be exchanged with the rotational direction of the hydraulic pump. Theoretically, the delivery flow rate is only dependent on the volumetric displacement and adjusted rotational speed. The smaller volumetric displacement corresponds to the higher resolution, and the minimum rotational speed corresponds to the critical suction flow capacity.

The hydraulic pump is driven by the electric servo motor, whose rotation speed experiences deviation due to the mechanical hysteresis. The Prandtl–Ishlinskii (PI) model is applied to model this mechanical hysteresis, and its inverse is incorporated into the feedforward module to compensate for the hysteresis. The PI model is derived from the weighted accumulation of a series of backlash operators and given by

$$n_p(t) = au(t) + bu^2(t) + W^T H_r[u, n_{p0}](t), \tag{5}$$

$$n_p(t) = W^T H_r[u, n_{p0}], \tag{6}$$

$$H_r[u, n_{p0}] = \max\{u(t) - r_i, \min[u(t) + r_i, n_{pi}(t - T)]\} \tag{7}$$

where u is the input excitation voltage, n_p is the rotation speed, and n_{p0} is the rotational speed at the initial time, a, b are constant coefficients. $W^T = [w_1, w_2, \ldots, w_n]$ is the weight matrix; $0 < r_1 < r_2 < \ldots < r_n$ is the threshold value. Based on the experimental results, relying on the least squares method, the unknown parameters of the PI hysteresis model are identified. Based on the PI model, the comparison of measured rotation speed and predicted rotation speed under the different driving voltages is depicted in Fig. 4(a).

As demonstrated in Fig. 4(a), the predicted rotation speed is within agreement with the measured rotation speed, and the mean absolute error is less than 5%. To eliminate the mechanical hysteresis between the measured rotation speed and driving voltage, the feedforward compensation based on the inverse PI hysteresis model is applied, and the comparison between the measured rotation speeds with inversed PI feedforward compensation and those without inversed PI feedforward compensation is depicted in Fig. 4(b).

As illustrated in Fig. 4(b), an amplitude of 1000 rpm and a frequency of 1 Hz sine curve are selected as the target rotation speed. With the inversed PI feedforward compensation, the rotation speed fluctuation is within 10 rpm regardless of the interference signal, and the time delay between the measured and target rotation speed is greatly reduced.

Except for the rotation speed, the error between the actual and given delivery flow rates of the hydraulic pump is also dependent on the load pressure and leakage, and the leakage can be estimated by using the measured results. Based on the compensated rotation speed, the pump volumetric flow rate q_{ps} is also determined by the leakage associated with the pressure differential and represented by the equation as

$$q_{ps} = n_p D_p - \Delta q_e = n_p D_p - k_p \Delta p_p, \tag{8}$$

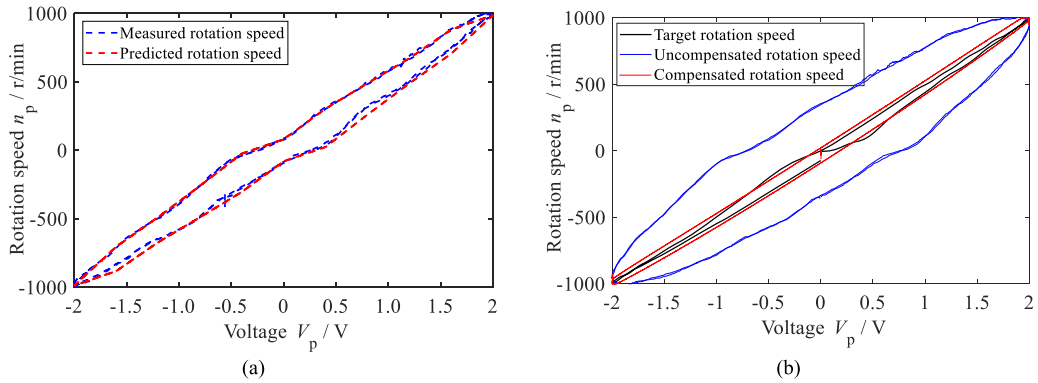

FIG. 4. (a) Validation of the PI hysteresis model. (b) Compensation of rotation speed.

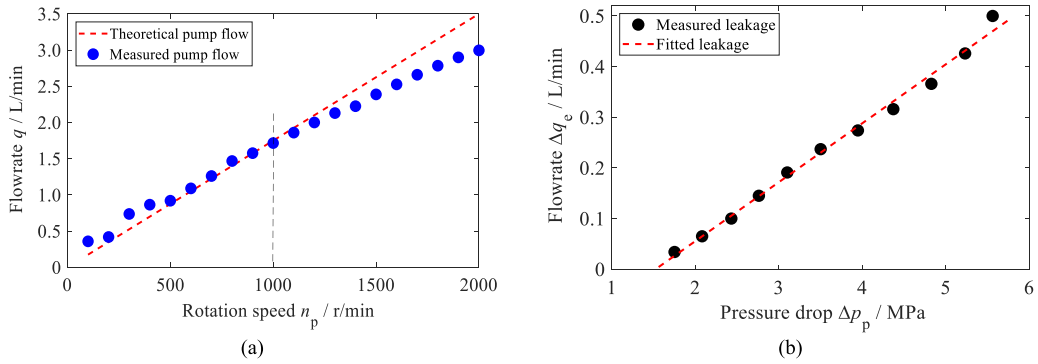

FIG. 5. (a) Comparison of theoretical and measured pump flow at the different rotation speeds. (b) Comparison of theoretical and measured pump flow at the different pressure drops.

where D_p is the displacement of the pump and n_p is the rotation speed of the electric servo motor. Δq_e is the leakage flow rate, and k_p is the leakage coefficient caused by the pressure drop Δp_p between the discharge port and suction port. The comparison between theoretical volumetric pump flow and measured pump flow is presented in Fig. 5(a). Besides, the leakage dependent on the pressure differential is fitted by the linear correlation and plotted in Fig. 5(b).

As demonstrated in Fig. 5, beyond the rotation speed of 1000 rpm, the difference between the theoretical pump flow and measured pump flow is determined by the leakage dependent on the pressure differential, and the leakage has a linear correlation with the pressure differential. The fitted curve is in agreement with the measured leakage, and the mean error is less than 3%. The accuracy of pump flow is the premise to ensure the accuracy of EHA position control.

B. Bypass digital flow circuit

The bypass digital flow circuit uses an accumulator to act as a flow rate source and two 2/2 way digital on–off valves and two check valves to eliminate flow asymmetry.

1. Modeling of digital on–off valve

The digital on–off valve is comprised of an armature, static iron, push rod, excitation coil, valve body, ball valve, return spring, and valve seat, as shown in Fig. 6.

The digital on–off valve couples electromagnetic, mechanic, and fluidic fields with mechanical energy conversion and dissipation. The performance of a digital on–off valve controlled by a PWM (Pulse Width Modulation) signal is subjected to the electromagnetic force, fluid-dependent force, and spring force. When the drive voltage is exerted on the electromagnetic coil, the generated magnetic field enables the ball valve to separate from the valve seat, and the supply flow is connected. When the electromagnetic coil is de-energized, the ball valve returns to the valve seat due to the reduced electromagnetic force rapidly. Here, neglecting the dynamics of the digital on–off valve, assuming it can open and close normally at a controlled duty cycle range.

The delivery flow rates of the 2/2 way digital on–off valves are modeled by using the conventional turbulent flow equation as follows:

$$q_{sv1} = \text{sign}\,(p_{pA} - p_{Acc})\tau_{s1} C_{dv} A_{jmax} \sqrt{\frac{2}{\rho}(p_{pA} - p_{Acc})}, \quad (9)$$

$$q_{sv2} = \text{sign}\,(p_{pa} - p_{Acc})\tau_{s2} C_{dv} A_{jmax} \sqrt{\frac{2}{\rho}(p_{pa} - p_{Acc})}, \quad (10)$$

where τ_{s1}, τ_{s2} are the duty cycles of digital on–off valves located at the piston-side and rod-side cylinder chambers, respectively; q_{sv1} and q_{sv2} are their flow rates of digital on–off valves at the maximum opening, p_{Acc} is the inlet pressure of the accumulator, ρ is the fluid density, and p_{pA}, p_{pa} are the upstream pressures of the piston-side and rod-side digital on–off valves, respectively; C_{dv} is the discharge

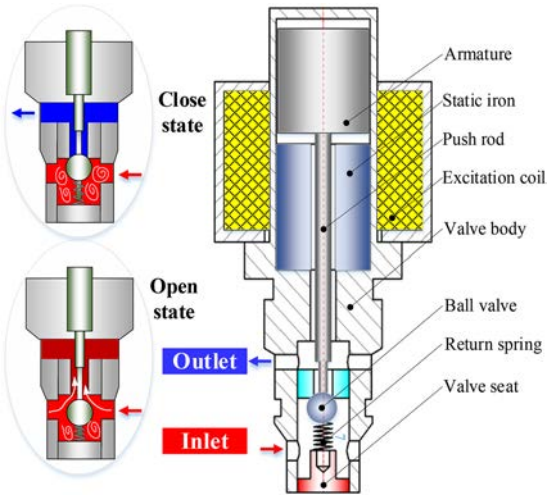

FIG. 6. Schematic diagram of a 2/2 way solenoid digital on–off valve.

coefficient, and A_{jmax} is the maximum opening of the digital on–off valve, which can be listed as

$$A_{jmax} = \pi x_{smax} \sin 2\alpha_0 \left(\frac{d_v}{2} + \frac{1}{2} x_{smax} \sin \alpha_0 \right), \quad (11)$$

where α_0 is the contact angle of the valve seat, d_v is the diameter of the ball valve, and x_{smax} is the stroke of the ball valve, and this is given in the supplier design handbook. Based on Eq. (11), the maximum opening of the digital on–off valve can be acquired. Besides, the discharge coefficient is subjected to the flow state and pressure drop and can be expressed by the equation as

$$C_{ds} = C_{dsmax} \tanh\left(\frac{2\mathrm{Re}}{\mathrm{Re}_{tr}}\right), \quad (12)$$

$$\mathrm{Re} = \frac{d_h}{v_f} \sqrt{\frac{2(p_0 - p_{d0})}{\rho}}, \quad (13)$$

where v_f is the kinematic viscosity of hydraulic oil, d_h is the equivalent hydraulic diameter, Re is the Reynolds number, and Re_{tr} is the critical Reynolds number. The delivery flow rates of digital on–off valves at the different duty cycles are presented in Fig. 7.

As demonstrated in Fig. 7, the linear correlation between the duty cycle and delivery flow rate is found during the duty cycle (0.1–0.9). The flow rate at the maximum opening is 2.5 l/min and is higher than the discharge pump flow with a rotation speed of 1000 rpm.

According to the principle of four quadrants, the discharge pressure p_{pA} and suction pressure p_{pa} in the first and third quadrants are described by

$$p_{pA} = \frac{K_e}{V_{dp}} \int [n_p D_p \operatorname{sign}(n_p) + q_{cv1} - q_{sv1} - q_p \operatorname{sign}(v_p)]\, dt, \quad (14)$$

$$p_{pa} = \frac{K_e}{V_{sp}} \int [q_a \operatorname{sign}(v_p) + q_{cv2} - q_{sv2} - n_p D_p \operatorname{sign}(n_p)]\, dt, \quad (15)$$

where V_{dp} and V_{sp} are the discharge and suction volumes, respectively. q_p is the flow rate entering the piston-side cylinder chamber, q_a is the flow rate getting out of the rod-side cylinder chamber, and K_e is the effective bulk modulus of the fluid. Similarly, the discharge pressure p_{pA} and suction pressure p_{pa} in the second and fourth quadrants can be given by the equation

$$p_{pA} = \frac{K_e}{V_{dp}} \int [q_{cv1} - q_{sv1} - q_p \operatorname{sign}(v_p) + q_m \operatorname{sign}(v_p)]\, dt, \quad (16)$$

$$p_{pa} = \frac{K_e}{V_{sp}} \int [q_a \operatorname{sign}(v_p) + q_{cv2} - q_{sv2} - q_m \operatorname{sign}(v_p)]\, dt, \quad (17)$$

where q_m is the flow rate across the separated hydraulic motor.

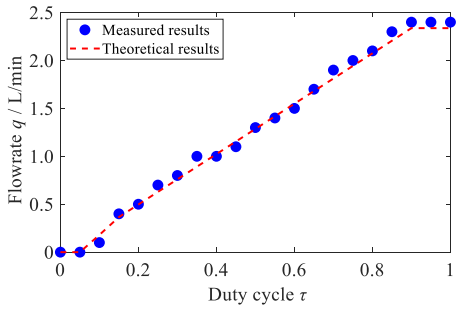

FIG. 7. Delivery flow rates of digital on–off valve.

2. Modeling of check valve

As a flow compensation component, the check valve is passively actuated by the pressure difference across it, which is subjected to the spring pre-compression and hydraulic forces. Its function is to permit flow in the positive direction and block it in the opposite direction. The delivery flow rate across the check valves can be modeled by

$$q_{cv1} = C_{dc} A_{cv} \sqrt{\frac{2}{\rho}(p_{leak} - p_{pA})} = C_{dc} A_{cv} \sqrt{\frac{2}{\rho} \Delta p_{cv1}}, \quad (18)$$

$$q_{cv2} = C_{dc} A_{cv} \sqrt{\frac{2}{\rho}(p_{leak} - p_{pa})} = C_{dc} A_{cv} \sqrt{\frac{2}{\rho} \Delta p_{cv2}}, \quad (19)$$

where C_{dc} is the discharge coefficient and A_{cv} is the effective opening area of the check valves, and they can be obtained by using the methodology of solving the maximum opening and discharge coefficient of the digital on–off valve. p_{leak} is the generated pressure at the upstream volume of the check valves and given by the equation

$$p_{leak} = \frac{K_e}{V_{leak}} \int (k_p \Delta p_p - q_{cv1} - q_{cv2})\, dt, \quad (20)$$

where V_{leak} is the upstream volume of the check valves. Assuming the state of the check valve switches instantaneously, the effective flow area A_{cv} increases linearly, ranging from the cracking pressure p_{cr} to the fully open pressure p_{or}. This relationship is quantified by the equation as

$$A_{cv} = \begin{cases} 0 \Delta p_{cv} < p_{cr}, \\ \dfrac{\Delta p_{cv} - p_{cr}}{p_{or}} A_{cmax} p_{cr} \le \Delta p_{cv} \le p_{cr} + p_{or}, \\ A_{cmax} \Delta p_{cv} > p_{cr} + p_{or}, \end{cases} \quad (21)$$

where p_{cr} is the cracking pressure, p_{or} is the override pressure, and A_{cmax} is the maximum effective flow area.

C. Actuation circuit

The actuation circuit includes a hydraulic cylinder and hydraulic motor; the characteristics of the hydraulic cylinder are determined by the pressure differential and state of the hydraulic motor.

1. Modeling of hydraulic cylinder

The asymmetric hydraulic cylinder linearly turns hydraulic power into mechanical power. The volumes of the piston chamber V_p and rod chamber V_a are defined as

$$V_p = V_{p0} + A_p x_p, \quad (22)$$

$$V_a = V_{a0} + \alpha A_p(x_{pmax} - x_p), \tag{23}$$

where x_p is the displacement of the piston, x_{pmax} is the stroke length of the piston, and V_{p0} and V_{a0} are the initial volume of the piston-side and rod-side cylinder chamber, respectively. The transient pressures in the cylinder chambers (piston side and rod side) are calculated by the flow continuity equation and can be given by the equations

$$\frac{dp_p}{dt} = \frac{K_e}{V_p}\left[q_p \operatorname{sign}(v_p) - A_p\frac{dx_p}{dt} - k_{cl}(p_p - p_a)\operatorname{sign}(p_p - p_a)\right], \tag{24}$$

$$\frac{dp_a}{dt} = \frac{K_e}{V_a}\left[-q_a \operatorname{sign}(v_p) + \alpha A_p\frac{dx_p}{dt} + k_{cl}(p_p - p_a)\operatorname{sign}(p_p - p_a)\right], \tag{25}$$

where k_{cl} is the internal leakage coefficient. The dynamic equilibrium of a cylinder piston can be given by the equation

$$m_p\frac{d^2x_p}{dt^2} + b_p\frac{dx_p}{dt} = (p_p - \alpha p_a)A_p - F_{cf} - F_e, \tag{26}$$

where m_p is the mass of the cylinder piston and b_p is the damping coefficient. The nonlinear friction force F_{cf} is measured with a constant velocity and can be represented by

$$F_{cf} = \left[F_{cp} + (F_{sp} - F_{cp})e^{-|v_p/v_s|}\right]\operatorname{sign}(v_p) + \sigma_2 v_p, \tag{27}$$

where F_{cp} is the Coulomb friction, F_{sp} is the maximum static friction, σ_2 is the viscous coefficient, and v_s is the characterized Stribeck velocity.

2. Modeling of hydraulic motor

The separated hydraulic motor is applied to translate the hydraulic energy to mechanical energy, avoiding the extra throttling dissipation that occurred at the digital on–off valve in the assistive quadrants. The dynamic equilibrium of the hydraulic motor in the second and fourth quadrants can be represented by the equation

$$(p_m - p_{Acc})D_m = I_m\frac{d\omega_m}{dt} + B_m\omega_m + F_{mf}, \tag{28}$$

TABLE I. Main parameters of the EHA theoretical model.

No.	Symbol	Quantity	Value
1	D_p	Displacement of pump	1.75×10^{-6} m^3/r
2	D_m	Displacement of hydraulic motor	1.75×10^{-6} m^3/r
3	I_m	Inertia moment of hydraulic motor	0.01 kg m^2
4	F_{sp}	Maximum static friction force	50 N
5	F_{cp}	Coulomb friction force	10 N
6	v_s	Characterized Stribeck velocity	0.5 m/s
7	σ_2	Viscous coefficient	10 N·s/m
8	F_{ms}	Maximum static friction force	20 N
9	F_{mc}	Coulomb friction force	5 N
10	ω_{m01}, ω_{m02}	Static friction reference velocities	10, 20 rad/s
11	B_m	Damping coefficient	0.8 N·s/rad
12	p_{cr}	Cracking pressure	0.3 MPa
13	p_{or}	Override pressure	0.5 MPa
14	V_{dp}	Discharge volume	7.23×10^{-4} m^3
15	V_{sp}	Suction volume	7.46×10^{-4} m^3
16	V_{p0}	Initial piston-side volume	5.88×10^{-5} m^3
17	V_{a0}	Initial rod-side volume	7.06×10^{-4} m^3
18	m_p	Mass of piston	0.46 kg
19	b_p	Damping coefficient	10 N·s/m
20	C_{dv}	Discharge coefficient	0.65
21	A_p	Piston area	7.46×10^{-4} m^3
22	k_{cl}	Leakage coefficient	1×10^{-12} L/min/Pa
23	K_e	Bulk modulus	3×10^8 Pa
24	A_{cmax}	Maximum flow area	2.5×10^{-6} m^2
25	k_p	Proportional coefficient	0.95
26	A_{jmax}	Maximum flow area	1.12×10^{-6} m^2
27	x_{pmax}	Maximum stroke of piston	175 mm
28	A_p	Piston-side area	7.07×10^{-4} m^2
29	α	Piston-ride and rod-side area ratio	0.64

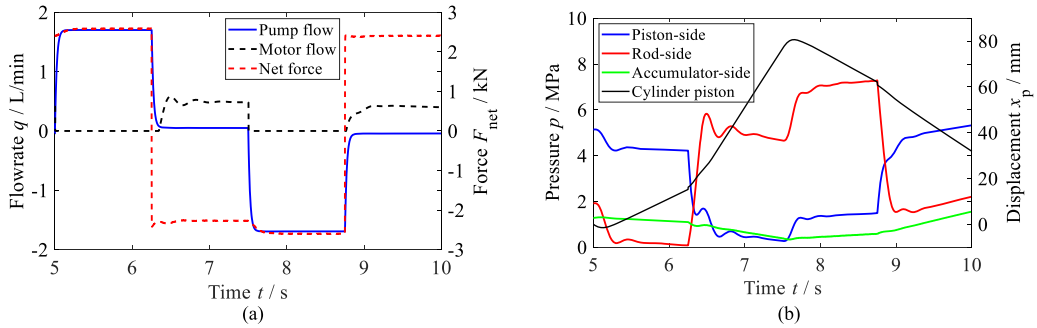

FIG. 8. (a) Pump flow, motor flow, and net force. (b) Chamber pressures and cylinder piston displacement.

$$p_m = \begin{cases} p_p\,(p_p - \alpha p_a)A_p > 0, \\ p_a\,(p_p - \alpha p_a)A_p < 0, \end{cases} \tag{29}$$

where I_m is the inertia moment of the hydraulic motor, D_m is the displacement of the hydraulic motor, ω_m is the angular speed of the hydraulic motor, B_m is the damping coefficient, and F_{mf} is the nonlinear friction, which can be expressed by

$$F_{mf} = \tanh\left(\frac{\omega_m}{\omega_{m01}}\right)\left[F_{mc} + (F_{ms} - F_{mc})e^{-\left(\frac{\omega_m}{\omega_{m02}}\right)}\right], \tag{30}$$

where F_{mc} is the coulomb friction force, F_{ms} is the maximum static friction force, and ω_{m01}, ω_{m02} are the static friction reference velocities. The accumulator inlet pressure p_{Acc} is determined by the flow rate of the digital on–off valves and the hydraulic motor output flow rate as given by

$$p_{Acc} = \frac{K_e}{V_{Acc} + V_{c0}} \int [n_m D_m + q_{sv1} + q_{sv2}]\,dt, \tag{31}$$

where V_{c0} is the initial volume of the inlet accumulator and n_m is the rotation speed of the hydraulic motor. The main parameters of the EHA theoretical model are listed in Table I.

IV. DISCUSSION OF EHA PERFORMANCE

The performance of EHA is significantly affected by the selected operating parameters; hence, parameter identifications are conducted to implement the four quadrant functionality.

A. EHA performance discussion

Based on the overall theoretical model of the proposed EHA, its main performance is evaluated in this section. When the proposed EHA is operated in the four quadrants, the calculated cylinder chamber pressures and cylinder piston displacement are depicted in Fig. 8.

As demonstrated in Fig. 8(a), the amplitude of generated pump flow is 1.7 L/min, the amplitude of leakage flow is 0.05 L/min, the amplitude of generated hydraulic motor flow is 0.5 L/min, and the net force exerted on the cylinder piston is consistent with the given external force. As illustrated in Fig. 8(b), under the given pump flow of 1.7 /min and external force of 2500 N, the cylinder piston periodically extends and retracts, experiencing positive and negative pressure differences. In the first quadrant, the piston-side cylinder chamber is pressurized to 4.3 MPa, and the cylinder piston linearly extends at a velocity of 15 mm/s. In the second quadrant, the cylinder piston maintains an extension velocity of 50 mm/s, and the rod-side cylinder chamber is passively pressurized to 4.9 MPa. In the third quadrant, the rod-side cylinder chamber is pressurized to 7.2 MPa, and the piston linearly retracts with a velocity of 20 mm/s. In the fourth quadrant, the cylinder piston maintains a retraction velocity of 22 mm/s, and the piston-side cylinder chamber is passively pressurized to 5.1 MPa.

To declare the flow capability of the separated hydraulic motor in the assistive quadrant, the delivery flow rates across the separated hydraulic motor at the different external forces are shown in Fig. 9.

As demonstrated in Fig. 9, when the external force is from 0.2 to 3.8 kN, the delivery flow rate across the separated hydraulic motor in the second quadrant linearly increases from 0.019 l/min to 0.56 l/min, and the slope is 0.15 l/min/kN. Meanwhile, the delivery flow rate across the separated hydraulic motor in the fourth quadrant linearly increases from 0.012 l/min to 0.43 l/min, and the slope is 0.12 l/min/kN. The discrepancy of flow rate gradient in the second and fourth quadrants is attributed to the differential pressure drop between the piston-side and rod-side cylinder chambers. Based on the flow rate slope in the fourth quadrant and asymmetric action area, the flow rate slope should be 0.18 l/min/kN, whereas the calculated flow slope is 0.12 l/min/kN, and the difference of 0.06 l/min/kN is due to the insufficient flow

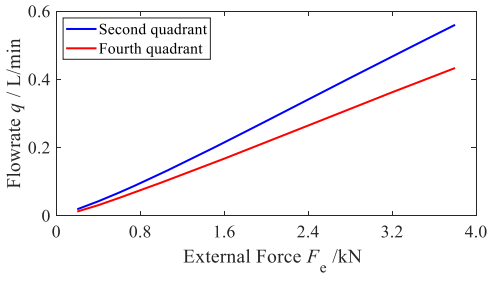

FIG. 9. Delivery flow rate in the assistive quadrant.

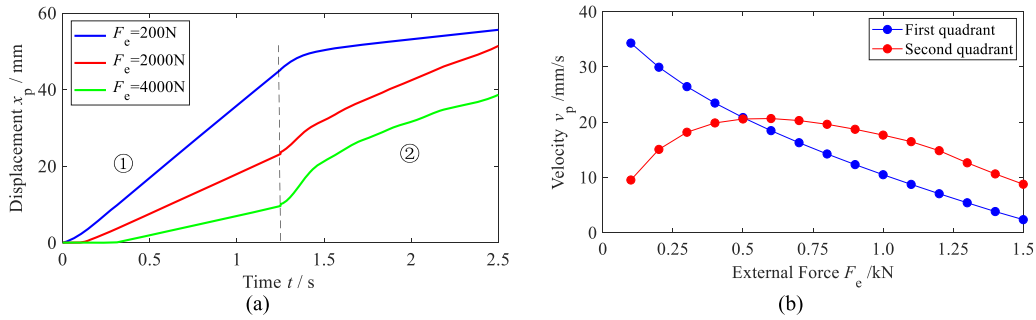

FIG. 10. (a) Displacement of cylinder piston in the extensive quadrant. (b) Motion velocity of cylinder piston in the extensive quadrant.

compensation dependent on the asymmetry action area of the hydraulic cylinder.

To evaluate the effect of the external force on the EHA performance, the transient displacement and its motion velocity of the cylinder piston in the extensive quadrant are depicted in Fig. 10.

As demonstrated in Fig. 10(a), in the first quadrant, the motion velocity of the cylinder piston decreases with the increase of external force. Under the external force of 0.2 and 4 kN, the motion velocities of the cylinder piston are 37.8 mm/s and 10.1 mm/s, respectively. In the second quadrant, the motion velocity of the cylinder piston increases with the increase of external force. Under the external force of 0.2 and 4 kN, the motion velocities of the cylinder piston are 5.7 mm/s and 20.6 mm/s, respectively. As depicted in Fig. 10(b), the motion velocity of the cylinder piston in the first quadrant linearly decreases with the increase of external force with a slope of 22.9 mm/s/kN. The motion velocity of the cylinder piston in the second quadrant first increase to a peak at the external force of 0.6 kN, then decreases with the increase of the external force with a slope of 15.4 mm/s/kN. The motion velocities of the cylinder piston intersect at the external force of 0.5 kN in the first and second quadrants. To evaluate the effect of the separated hydraulic motor on the EHA performance in the extensive quadrant, the displacement of the cylinder piston, dissipated power (represented by the products of the pressure difference and delivery flow) across the rod-side digital on–off valve (FSV02), and translated power (represented by the products of the pressure drop and delivery flow) that occurred at the separated hydraulic motor are depicted in Fig. 11.

As demonstrated in Fig. 11(a), in the second quadrant, the EHA without separated hydraulic motor exhibits a larger extensive motion velocity of the cylinder piston compared with the electro-hydrostatic actuator with separated hydraulic motor (EHA-SHM), and their motion velocities are 52 mm/s and 45.3 mm/s, respectively. During the transition period, the actuator experiences from reverse load to forward load, and the forward load is far greater than the resistive force caused by fluid compressibility in the rod-side cylinder chamber. Meanwhile, the consistency of the forward load and the direction of the piston motion lead to a larger acceleration in the initial stage of the second quadrant. As the piston extends, the rod-side cylinder chamber becomes smaller, the rod-side cylinder chamber pressure gradually increases, and the acceleration decreases. These are mainly responsible for the phenomenon that the motion velocity of the cylinder piston in the second quadrant first increases and then decreases. As demonstrated in Fig. 11(b), in the second quadrant, the dissipated power occurred at the rod-side digital on–off valve and translated power across the separated hydraulic motor nonlinearly varied with the growth of external force, and their maximum values are 59.8 and 122.5 W, respectively. The separated hydraulic motor enables EHA to exhibit 104% energy recuperation compared with EHA without SHM in the second quadrant. Besides, the separated hydraulic motor has better adaptability to the greater external force, and the larger power is translated to kinetic energy.

To evaluate the effect of the external force on the EHA performance, the transient displacement and its motion velocity of the cylinder piston in the retractive quadrant are depicted in Fig. 12.

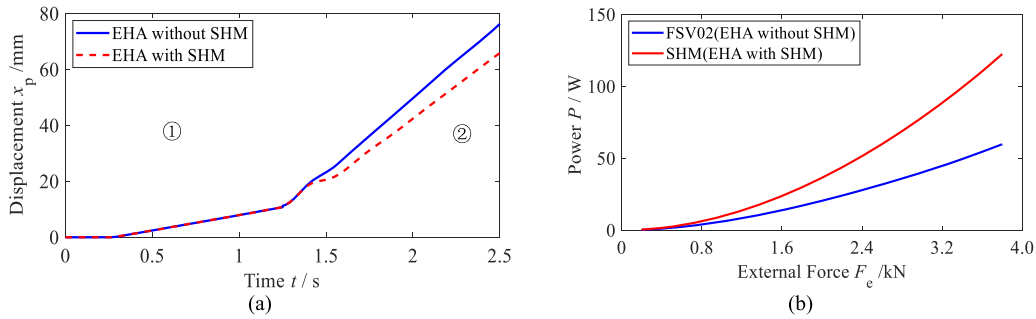

FIG. 11. (a) Displacement of cylinder piston. (b) Dissipated power and translated power.

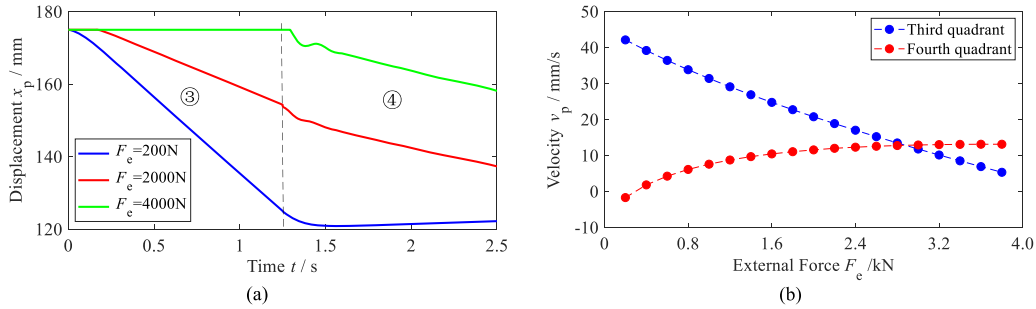

FIG. 12. (a) Displacement of cylinder piston in the retractive quadrant. (b) Motion velocity of the cylinder piston in the retractive quadrant.

As demonstrated in Fig. 12(a), in the third quadrant, the motion velocity of the cylinder piston decreases with the increase of external force. Under the external force of 0.2 and 4 kN, the motion velocities of the cylinder piston are 42 mm/s and zero, respectively. In the fourth quadrant, the motion velocity of the cylinder piston increases with the increase of external force. Under the external force of 0.2 and 4 kN, the motion velocities of the cylinder piston are −0.8 and 12.8 mm/s, respectively. As depicted in Fig. 12(b), the motion velocity of the cylinder piston in the third quadrant linearly decreases with the increase of external force with a slope of 10.2 mm/s/kN. The motion velocity of the cylinder piston in the fourth quadrant nonlinearly increases before the external force of 0.4 kN, then linearly increase with the increase of the external force with a slope of 1.21 mm/s/kN, and the motion velocities of the cylinder piston in the third and fourth quadrants cross at the external force of 2.8 kN. Due to the asymmetric action area, the insufficient flow compensation is responsible for the asymmetric law of cylinder piston motion velocity in the extensive quadrant.

To evaluate the effect of the separated hydraulic motor on the EHA performance in the retractive quadrant, the displacement of the cylinder piston, dissipated power (represented by the products of the pressure difference and delivery flow) across the piston-side digital on–off valve (FSV01), and translated power (represented by the products of the pressure drop and delivery flow) that occurred at the separated hydraulic motor are depicted in Fig. 13.

As shown in Fig. 13(a), in the fourth quadrant, the EHA without a separated hydraulic motor has a larger retractive motion velocity of the cylinder piston compared with the EHA-SHM, and their motion velocities are 28.5 and 21.2 mm/s, respectively. As demonstrated in Fig. 13(b), in the fourth quadrant, the dissipated power occurred at the piston-side digital on–off valve and translated power across the separated hydraulic motor nonlinearly varied with an increase of external force, and their maximum values are 45.6 and 62.3 W. The separated hydraulic motor enables EHA to have 36.7% energy recuperation compared with EHA without SHM in the fourth quadrant.

B. Four quadrants division

The four quadrants division aims at classifying the working conditions of the proposed EHA. Unfortunately, the existing four quadrants division method simply considers that the pressure difference between the piston-side chamber pressure p_p and rod-side chamber pressure p_a is consistent with the direction of external force, neglecting the pressure instability caused by insufficient flow compensation. As described in the section of operational quadrants of EHA, using the proposed four quadrants division methodology incorporated into the theoretical model, judge the current operational quadrant of EHA, avoiding the existing misjudgment issue.

To declare the difference between the existing four quadrant division method and the proposed four quadrant division method, the net force exerted on the hydraulic cylinder at the different external forces acts as a significant evaluation index. Under the given external force of 0.2 and 0.8 kN, the calculated net forces exerted on the cylinder piston by using existing and proposed four quadrant division methods are depicted in Fig. 14.

As demonstrated in Fig. 14(a), when the EHA experiences the given external force of 0.2 kN in the resistive quadrant, the calculated net forces by the existing and proposed four quadrant division

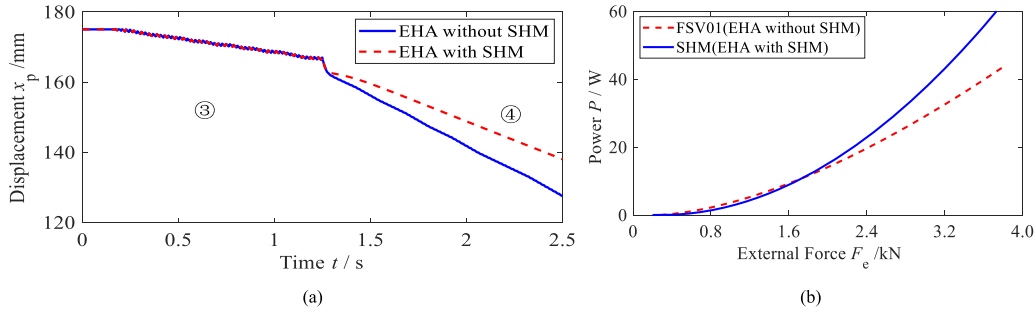

FIG. 13. (a) Displacement of cylinder piston in the retractive quadrant. (b) Dissipated power in the retractive quadrant.

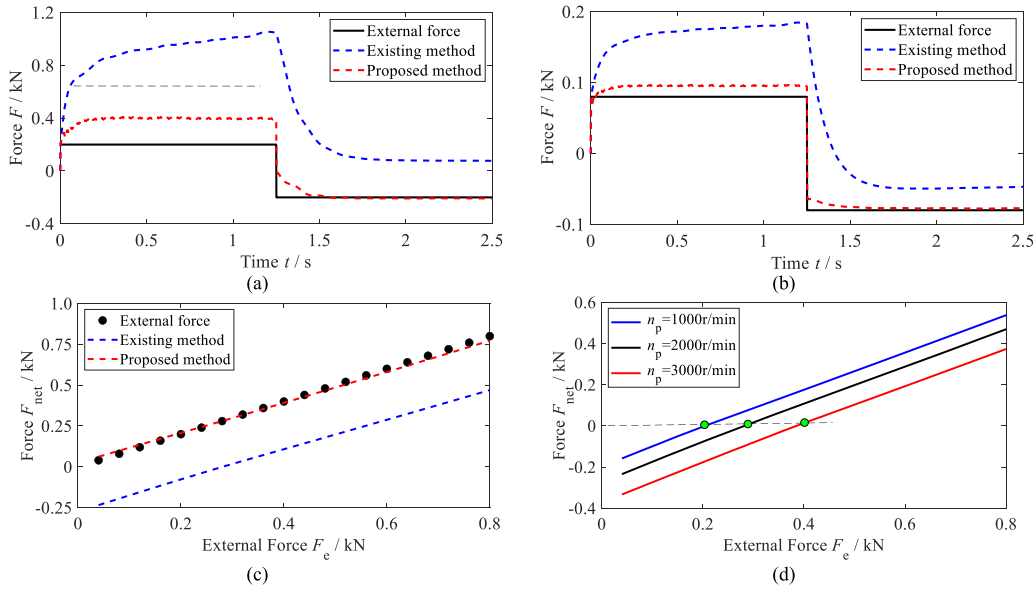

FIG. 14. (a) Comparison of net force at the external force 200 N. (b) Comparison of net force at the external force 800 N. (c) Comparison of net force at different external force. (d) Prediction of net force at different rotation speed.

method are 970 and 402 N, respectively, and the calculated net force is consistent with the direction of the given external force. The calculated positive difference between the calculated net force and the given force is attributed to the nonlinear friction. When the EHA experiences the given external force of −0.2 kN in the assistive quadrant, the calculated net force by using the existing and proposed four quadrant division methods is 80 and −206 N, respectively. The net force calculated by the proposed four quadrant division method is consistent with the direction of the external force, while the net force calculated by the existing four quadrant division method is

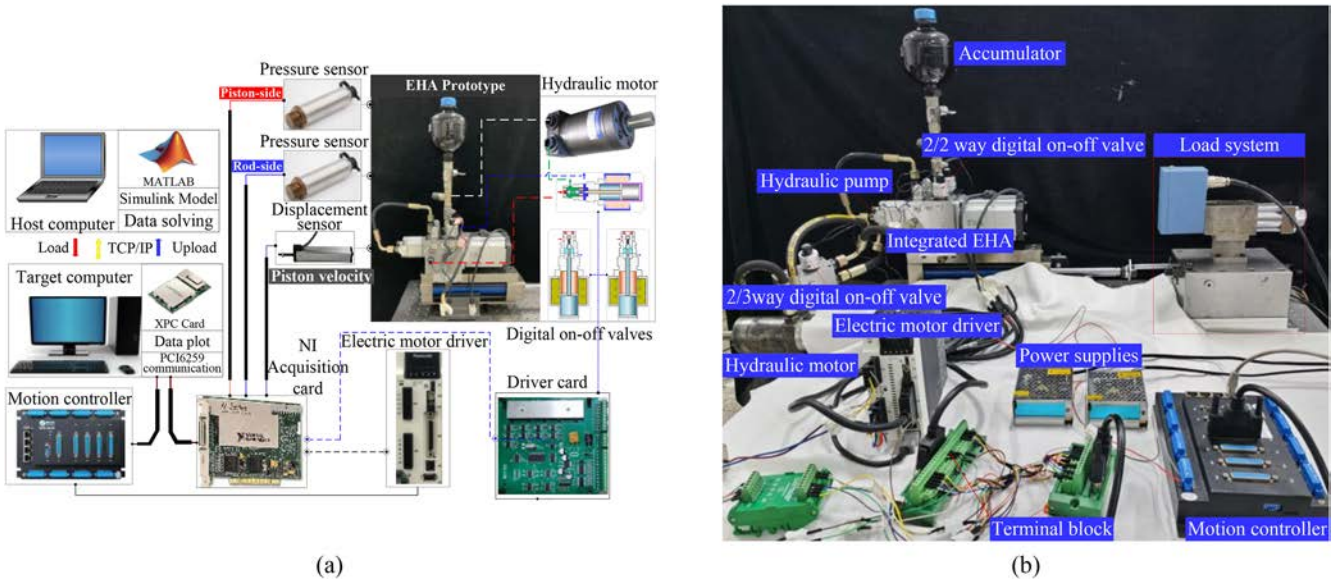

FIG. 15. (a) Test rig diagram of proposed EHA. (b) Test rig photograph of proposed EHA.

opposite to the direction of the external force. This misjudgment easily causes the inconsistent flow control of the digital on–off valve. As illustrated in Fig. 14(b), either EHA experiences the given external force of 0.08 kN or the given external force of −0.08 kN; the acquired net force calculated by the proposed four quadrant division method and existing four quadrant division method are consistent with the given external force. This indicated that the misjudgment derived from the existing four quadrant division is subjected to a threshold value. As demonstrated in Fig. 14(c), the calculated net force in the assistive quadrant linearly increases with the increase of external force, and the calculated net force by using the proposed four quadrant division method shows good agreement within the given external force, while the calculated net force by using the existing four quadrant division method is opposite to the direction of the given external force below 288 N, and this value is named as the critical net force. As demonstrated in Fig. 14(d), the critical net force calculated by the existing four quadrant division method linear varied with the growth of rotation speed. When the rotation speeds are 1000 and 3000 rpm, the critical external forces are 200 and 384 N, respectively. This indicated that the increased pump discharge flow affects the pressure in the cylinder chamber and expands the range of misjudgment of quadrants by using the existing four quadrant division method.

V. EXPERIMENTAL TEST OF EHA

To validate the theoretical model of proposed AEHA and evaluate the four quadrant functionality and novel four quadrant division method of proposed EHA configuration, the experimental tests of EHA are conducted in this section.

A. Experimental configuration

The test rig of the proposed EHA contains the integrated AEHA, driving, measurement apparatus, and auxiliary components, as shown in Fig. 15.

The integrated EHA consists of an electric servo motor with a rotation speed encoder, a servo driver, a bidirectional fixed-displacement hydraulic pump, a fixed-displacement hydraulic motor, a 2/3 way digital on–off valve, two 2/2 way digital on–off valves, two relief valves, two check valves, and an asymmetric hydraulic cylinder. The driving and measurement apparatus contains a RT-Link controller platform, a multi-voltage driver, two high-frequency response pressure sensors, a displacement sensor, a flowmeter, a motion controller, and several 24 V linear DC power supplies. The load system contains the direct drive servo valve and symmetrical hydraulic cylinder and acts as the equivalent loads. The pressure sensors and displacement sensors are applied to measure cylinder chamber pressures and cylinder piston displacement. The control signal is sent by the RT-Link controller platform. The main technical parameters of the utilized apparatus are listed in Table II.

B. Experimental validation

Based on the test rig of EHA, the transient pressure in the cylinder chambers and displacement of the cylinder piston are used to validate the theoretical model in this section.

TABLE II. Main apparatus of proposed integrated EHA.

No.	Apparatus	Supplier	Model	Technical parameter
1	Electric servo motor	Panasonic	MHMF082L1V2M	Rated power: 750 W, rated rotation speed: 3000 rev/min
2	Servo driver	Panasonic	MCDLT35SF	⋯
3	Hydraulic pump	Marzocchi	U0.5R1.00VN GKX	Displacement: 1.75 ml/rev, nominal speed: 1500 rev/min
4	2/3 way digital on–off valve	Guizhou, Honglin	HSV3102S3	Rated flow rate: 3–9 l/min, rated pressure: 10 MPa
5	2/2 way digital on–off valve	Guizhou, Honglin	HSV3101S3	Rated flow rate: 3–9 l/min, rated pressure: 10 MPa, Response: ≤3.5 ms
6	Relief valve	VIS	RVB7.S08.0S.000	Maximum flow rate: 25 l/min, maximum setting range: 1–16 MPa
7	Asymmetric hydraulic cylinder	Self-manufacture	⋯	Stroke: 175 mm, piston and rod diameter: 30 and 18 mm
8	RT-link controller platform	Beijing RT	⋯	NI acquisition card 6259
9	Multi-voltage driver	MATRIX	HSDB 990.012	16-Channel digital port
10	Pressure sensor	Kunshan Shuangqiao	CYG1401F	With a range of 0–10 MPa, accuracy: 0.5%
11	Displacement sensor	MIRAN	KTC1/LWH-175	Stroke: 175 mm, linearity: 0.1%
12	Flowmeter	Shanghai Yangji	FGR200/3L	Range: 0.1–3 l/min, Accuracy: ±0.5%
13	Motion controller	LEADSHINE	SMC304-BAS	Resolution: ±0.1 Hz
14	24 V linear DC power suppliers	Chaoyang power	4NIC-X24	Output voltage: 24 V, resolution: ±1%
15	Symmetrical hydraulic cylinder	Self-manufacture		Stroke: 135 mm, piston and rod diameter: 30 and 10 mm

1. Resistive extension and assistive retraction

To prove the four quadrant functionality of the proposed EHA, the transient characteristics in two quadrants are used to investigate the EHA performance. These include the switching process between the resistive extension and assistive retraction (first and fourth quadrant), the resistive retraction and assistive extension (third and second quadrant), as well as the resistive retraction and resistive extension (third and first quadrant). The transient characteristics in the first and fourth quadrants are shown in Fig. 16.

As demonstrated in Fig. 16(a), the proposed EHA experiences resistive extension 0.8 s (20%) and assistive retraction 3.2 s (80%) during the 4 s period. In the first quadrant, the pump discharge flow enables the cylinder piston to extend resistively, and the velocity of the cylinder piston approaches 16.3 mm/s. As demonstrated in Fig. 16(b), the pressure at the piston-side cylinder chamber rises to 2.3 MPa, and the pressure at the rod-side cylinder chamber drops to 0.1 MPa. The calculated net force $[(p_p\text{-}\alpha p_a)A_p]$ is 1579.7 N and is consistent with the pressure difference $(p_p - p_a)$ of 2.2 MPa. In the fourth quadrant, the pump stops working, and the amplitude of 1200 N external force enables the cylinder piston to retract with a velocity of −16 mm/s. The pressure at the piston-side cylinder chamber drops to 1.4 MPa, and the pressure at the rod-side cylinder chamber rises to 1.0 MPa. The calculated net force $[(p_p\text{-}\alpha p_a)A_p]$ is 536.9 N and is consistent with the pressure difference $(p_p - p_a)$ of 0.4 MPa. The experimental results agree well with the theoretical results, which validates the accuracy of the theoretical model.

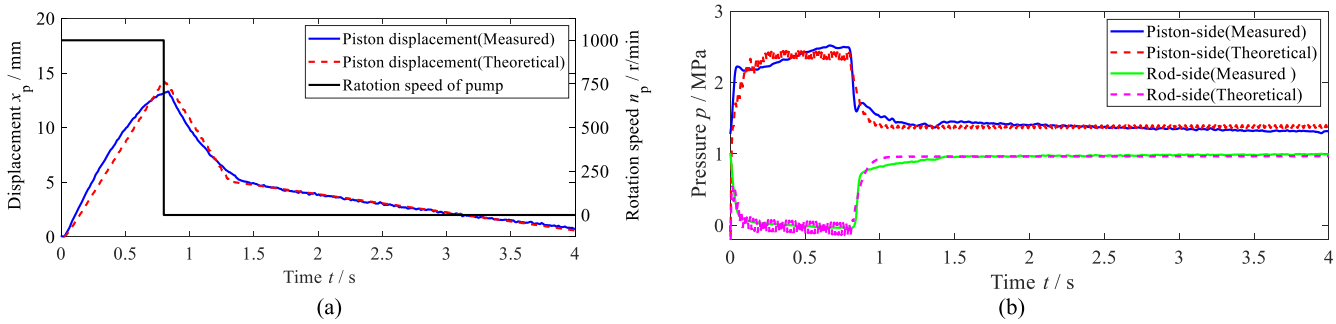

FIG. 16. (a) Transient displacement of cylinder piston in the first and fourth quadrants. (b) Transient pressures at the cylinder chambers in the first and fourth quadrants.

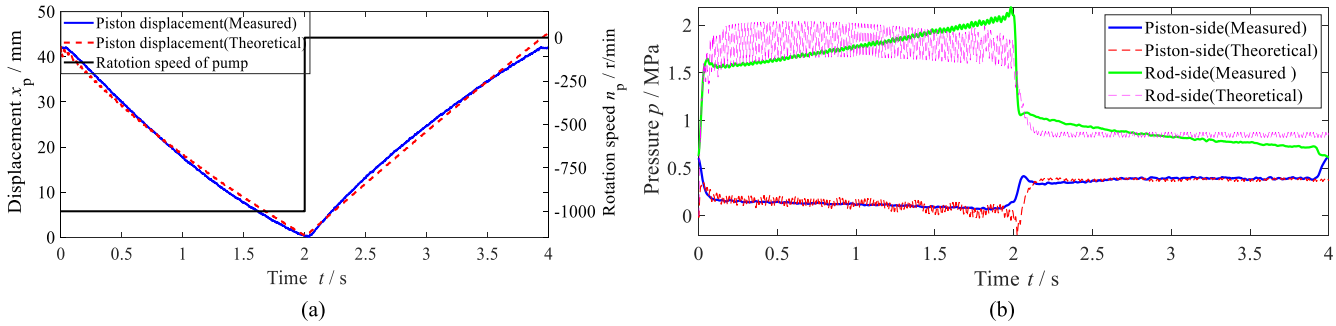

FIG. 17. (a) Transient displacement of cylinder piston in the third and second quadrants. (b) Transient pressure at the cylinder chambers in the third and second quadrants.

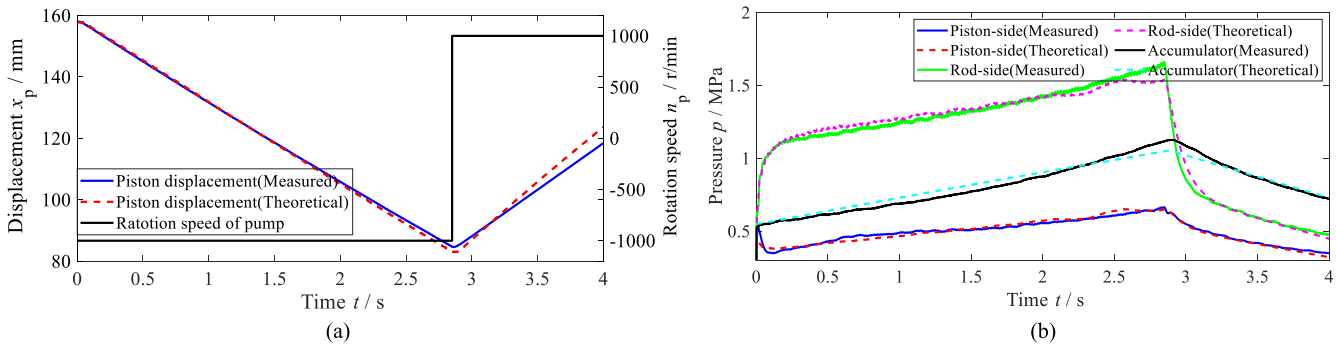

FIG. 18. (a) Transient displacement of cylinder piston in the third and first quadrants. (b) Transient pressures at the cylinder chambers in the third and first quadrants.

2. Resistive retraction and assistive extension

To declare transient characteristics in the third and second quadrants, the transient cylinder piston displacement and pressures at the cylinder chambers are shown in Fig. 17.

As demonstrated in Fig. 17(a), the proposed EHA experiences resistive retraction 2 s (50%) and assistive extension 2 s (50%) during the 4 s period. In the third quadrant, the reversed pump discharge flow drives the cylinder piston to retract resistively, and the velocity of the cylinder piston approaches −20 mm/s. As demonstrated in Fig. 17(b), the pressure at the piston-side cylinder chamber drops to 0.25 MPa, and the pressure at the rod-side cylinder chamber rises to 1.8 MPa. The calculated net force $[(p_p\text{-}\alpha p_a)A_p]$ is −637.3 N and is consistent with the pressure difference $(p_p - p_a)$ of −1.55 MPa. In the second quadrant, the pump stops working, and the amplitude of −1200 N external force enables the cylinder piston to extend with a velocity of 16 mm/s. The pressure at the piston-side cylinder chamber rises to 0.4 MPa, and the pressure at the rod-side cylinder chamber drops to 0.8 MPa. The calculated net force $[(p_p\text{-}\alpha p_a)A_p]$ is −79.1 N and is consistent with the pressure difference $(p_p - p_a)$ of −0.4 MPa.

3. Resistive retraction and resistive extension

Here, the transient characteristics in the first and third quadrants are investigated experimentally, and the measured and predicted cylinder piston displacement and transient pressures at the cylinder chambers are shown in Fig. 18.

As demonstrated in Fig. 18(a), the proposed EHA experiences resistive retraction 2.8 s (70%) and resistive extension 1.2 s (30%) during the 4 s period. In the third quadrant, the reversed pump discharge flow enables the cylinder piston to retract resistively, and the velocity of the cylinder piston approaches −26.7 mm/s. As demonstrated in Fig. 18(b), the pressure at the piston-side cylinder chamber increases from 0.4 to 0.5 MPa gradually, and the pressure at the rod-side cylinder chamber increases from 1.0 to 1.5 MPa. The inlet pressure at the accumulator ranges from 0.5 to 1 MPa, which is due to the revered pump discharged flow and the recuperated flow to the accumulator. The calculated net force $[(p_p\text{-}\alpha p_a)A_p]$ is −325 N and is consistent with the pressure difference $(p_p - p_a)$ of −1.0 MPa. In the first quadrant, the pump discharge flow enables the cylinder piston to extend with a velocity of 29.1 mm/s resistively. The pressure at the piston-side cylinder chamber decreases back to 0.4 MPa gradually, and the pressure at the rod-side cylinder chamber decreases from 1.5 to 0.5 MPa. The calculated net force $[(p_p\text{-}\alpha p_a)A_p]$ is 56.52 N and is opposite to the pressure difference $(p_p - p_a)$ of −0.1 MPa. The inlet pressure at the accumulator also ranges from 1 to 0.75 MPa, which is caused by the pump discharge flow and the compensated flow from the accumulator.

VI. CONCLUSION

The characteristics of the digital control four quadrants EHA with separated hydraulic motor were investigated in this article, and the main conclusions are drawn as follows:

(1) For the resistive quadrant, either extension or retraction, the increased external force causes the linearly reduced extension and retraction motion velocity of the cylinder piston and their slope of 22.9 mm/s/kN and 10.2 mm/s/kN, respectively. For the assistive extension and retraction quadrant, the linear reduction of the cylinder piston extension motion velocity above the external force of 0.5 kN with a slope of 15.4 mm/s/kN and the linear increase of the cylinder retraction motion velocity above the external force of 2.8 kN with a slope of 1.21 mm/s/kN are found. Due to the asymmetric action area, insufficient flow compensation and recuperation are responsible for the asymmetric motion velocity law of the cylinder piston.

(2) In the second quadrant, under the external force of 3.8 kN, the maximum dissipated occurred at the rod-side digital on–off valve, and translated power occurred at the SHM at 59.8 and 122.5 W, respectively. The cylinder piston motion velocities of EHA without SHM and EHA-SHM are 52 and 45.3 mm/s. In the fourth quadrant, the maximum dissipated occurred at the piston-side digital on–off valve, and translated power occurred at the SHM at 45.6 and 62.3 W, respectively. The cylinder piston motion velocities of EHA without SHM and EHA-SHM are 28.5 and 21.2 mm/s, respectively. Compared with EHA without SHM, the energy dissipation is reduced by 104% and 36.7%, respectively, while the motion velocity of the cylinder piston is reduced by 12.9% and 25.6%, respectively, in the second and fourth quadrants.

(3) The calculated net force by using the proposed four quadrant division method shows good agreement with the given external force in the assistive quadrant, while the calculated net force by the existing four quadrant division method is opposite to the direction of the given external force below the external force of 288 N. This critical net force varies from 200 to 384 N with the growth of rotation speed (ranges from 1000 to 3000 rpm) under the influence of resistive quadrants.

(4) The measured results indicated that the pressure difference of −1.0 MPa in the third quadrant enables EHA to experience a retraction motion velocity of 26.7 mm/s and a net force of −325 N. The pressure difference of −0.1 MPa in the first quadrant causes an extension motion velocity of 29.1 mm/s and a net force of 56.52 N and is consistent with the given external force. The calculated net force can effectively correct quadrant division determined by pressure difference. The discrepancy of motion velocity is 8.2%; the larger motion velocity can be obtained relying on less pressure difference in the assistive quadrant.

ACKNOWLEDGMENTS

The authors disclosed receipt of the following financial support for the research, authorship, and/or publication of this article: This work was supported by the National Natural Science Foundation of China (Grant Nos. 52375059 and 51975275) and the Primary Research & Development Plan of Jiangsu Province (Grant No. BE2021034).

AUTHOR DECLARATIONS

Conflict of Interest

The authors have no conflicts to disclose.

Author Contributions

Xiaoming Chen: Conceptualization (equal); Data curation (equal); Formal analysis (equal); Investigation (equal); Methodology (equal); Project administration (equal); Validation (equal); Writing – original draft (equal). **Yuchuan Zhu**: Conceptualization (equal); Formal analysis (equal); Funding acquisition (equal); Methodology (equal); Resources (equal); Supervision (equal); Validation (equal); Visualization (equal); Writing – review & editing (equal). **Jie Ling**: Methodology (equal); Project administration (equal); Supervision (equal); Validation (equal); Writing – review & editing (equal). **Mingming Zhang**: Investigation (equal); Project administration (equal); Validation (equal); Visualization (equal); Writing – review & editing (equal).

DATA AVAILABILITY

The data that support the findings of this study are available from the corresponding author upon reasonable request.

REFERENCES

[1]S. A. Ali, A. Christen, S. Begg, and N. Langlois, "Continuous–discrete time-observer design for state and disturbance estimation of electro-hydraulic actuator systems," IEEE Trans. Ind. Electron. **63**(7), 4314–4324 (2016).

[2]B. Németh, B. Varga, and P. Gáspár, "Hierarchical design of an electro-hydraulic actuator based on robust LPV methods," Int. J. Control **88**(8), 1429–1440 (2015).

[3]J. C. Maré, *Aerospace Actuators 2: Signal-by-Wire and Power-by-Wire* (John Wiley & Sons, 2017).

[4]R. Alden, "*Flight demonstration, evaluation and proposed applications for various all electric flight control actuation system concepts*," in *Proceedings of the Aerospace Design Conference* (AIAA, Big Sky, MT, 2013), p. 1171.

[5]B. Yang, Y. J. Lu, H. Y. Jiang, Z. F. Ling, T. Li, H. Liu, and X. P. Ouyang, "Quantitative comparative study on the performance of a valve-controlled actuator and electro-hydrostatic actuator," Actuators **13**(4), 118 (2024).

[6]J. C. Maré and J. Fu, "Review on signal-by-wire and power-by-wire actuation for more electric aircraft," Chin. J. Aeronaut. **30**(3), 857–870 (2017).

[7]J. J. Harris, "F-35 flight control law design, development and verification," in *2018 Aviation Technology, Integration, and Operations Conference* (AIAA, 2018), p. 3516.

[8]R. Kang, J. C. Mare, and Z. Jiao, "Nonlinear modelling and control design of electro-hydrostatic actuator," in *Proceedings of the 7th JFPS International Symposium on Fluid Power* (Japanese Fluid Power System Society, Toyama, Japan, 2008), pp. 665–670.

[9]K. R. McCullough, "Design and characterization of a dual electro-hydrostatic actuator," Ph.D. dissertation (McMaster University, Canada, 2011).

[10]Y. Zhang, Y. Fu, and W. Zhou, "Optimal control for EHA-VPVM system based on feedback linearization theory," in *Proceedings of the 11th International Conference on Control automation Robotics & Vision* (IEEE, Singapore, 2010), pp. 744–749.

[11]J. H. Kim and Y. S. Hong, "Comparison of force control characteristics between double-rod and single-rod type electro-hydrostatic actuators (I): Tracking performance," J. Drive Control **14**(4), 9–16 (2017).

[12]J. Yao, D. T. Jiang, W. Zhang, and Z. S. Dong, "First-order trajectory sensitivity analysis of open circuit pump controlled asymmetric cylinder systems," J. Mech. Eng. **55**(02), 223–232 (2019) (in Chinese).

[13]H. Zhao, H. J. Zhang, L. Quan, and B. Li, "Characteristics of asymmetrical pump controlled differential cylinder speed servo system," J. Mech. Eng. **49**(22), 170–176 (2013).

[14]J. Huang, H. Zhao, L. Quan, and X. Zhang, "Development of an asymmetric axial piston pump for displacement-controlled system," Proc. Inst. Mech. Eng., Part C **228**(8), 1418–1430 (2014).

[15]X. G. Zhang, L. Quan, Y. Yang, C. B. Wang, and L. W. Yao, "Theoretical analysis and experimental research on characteristics of parallel three assignment windows axial piston pump," J. Mech. Eng. **47**(14), 151–157 (2011).

[16]P. Achten, T. van den Brink, J. Potma, and M. Schellekens, "*A four-quadrant hydraulic transformer for hybrid vehicles*," in *Proceedings of the 11th Scandinavian International Conference on Fluid Power* (Linköping University Press, Linköping, Sweden, 2009), pp. 324–339.

[17]E. Busquets and M. Ivantysynova, "Discontinuous projection-based adaptive robust control for displacement-controlled actuators," J. Dyn. Syst., Meas., Control **137**(8), 081007 (2015).

[18]J. H. Huang, W. He, H. M. Hao, and L. Quan, "Analysis of control characteristics of variable-displacement asymmetric axial piston pump," Trans. Chin. Soc. Agric. Mach. **50**(3), 368–376 (2019) (in Chinese).

[19]J. Y. Oh, G. H. Jung, G. H. Lee, Y. J. Park, and C. S. Song, "Modeling and characteristics analysis of single-rod hydraulic system using electro-hydrostatic actuator," Int. J. Precis. Eng. Manuf. **13**(8), 1445–1451 (2012).

[20]L. Wang, W. J. Book, and J. D. Huggins, "A hydraulic circuit for single rod cylinders," J. Dyn. Syst., Meas., Control **134**(1), 011019 (2012).

[21]G. T. Bui, J. H. Wang, and J. L. Lin, "Optimization of micropump performance utilizing a single membrane with an active check valve," Micromachines **9**(1), 1 (2018).

[22]Q. Zhang, X. D. Kong, B. Yu, K. Ba, Z. Jin, and Y. Kang, "Review and development trend of digital hydraulic technology," Appl. Sci. **10**(2), 579 (2020).

[23]J. Yao, P. Wang, Z. S. Dong, D. T. Jiang, and T. Sha, "A novel architecture of electro-hydrostatic actuator with digital distribution," Chin. J. Aeronaut. **34**(5), 224–238 (2021).

[24]N. Alle, S. S. Hiremath, S. Makaram, K. Subramaniam, and A. Talukdar, "Review on electro hydrostatic actuator for flight control," Int. J. Fluid Power **17**(2), 125–145 (2016).

[25]G. Altare and A. Vacca, "A design solution for efficient and compact electro-hydraulic actuators," Procedia Eng. **106**, 8–16 (2015).

[26]D. Riu, M. Sautreuil, N. Rétière, and O. Sename, "Control and design of DC grids for robust integration of electrical devices. Application to aircraft power systems," Int. J. Electr. Power. Energy Syst. **58**, 181–189 (2014).

[27]Z. X. Jiao, Y. P. Li, T. Yu, C. F. Jiang, L. G. Huang, and Y. X. Shang, "Dynamic thermal coupling modeling and analysis of wet electro-hydrostatic actuator," Chin. J. Aeronaut. **35**(6), 298–311 (2022).

[28]J. H. Liu, H. Huang, Y. W. Ge, X. L. Zhao, W. X. Deng, G. G. Gao, and J. Y. Yao, "Thermal characteristic and analysis of electro-hydrostatic actuator," IEEE Access **12**, 34222–34234 (2024).

[29]J. A. Zhao, J. Fu, Y. C. Li, H. T. Qi, Y. Wang, and Y. Fu, "Flow characteristics of integrated motor-pump assembly with phosphate ester medium for aerospace electro-hydrostatic actuators," Chin. J. Aeronaut. **36**(9), 392–407 (2023).

[30]Y. Shang, X. Li, H. Qian, S. Wu, Q. Pan, L. Huang, and Z. Jiao, "A novel electro hydrostatic actuator system with energy recovery module for more electric aircraft," IEEE Trans. Ind. Electron. **67**(4), 2991–2999 (2020).

[31]S. Y. Qu, F. Zappaterra, A. Vacca, and E. Busquets, "An electrified boom actuation system with energy regeneration capability driven by a novel electro-hydraulic unit," Energy Convers. Manage. **293**(293), 117443 (2023).

[32]G. Koury Costa and N. Sepehri, "A critical analysis of valve-compensated hydrostatic actuators: Qualitative investigation," Actuators **8**(3), 59 (2019).

[33]G. K. Costa and N. Sepehri, "Four-quadrant analysis and system design for single-rod hydrostatic actuators," J. Dyn. Syst., Meas., Control **141**(2), 021011 (2019).

[34]S. Qu, D. Fassbender, A. Vacca, and E. Busquets, "A high-efficient solution for electro-hydraulic actuators with energy regeneration capability," Energy **216**, 119291 (2021).

[35]S. Y. Qu, D. Fassbender, A. Vacca, and E. Busquets, "A cost-effective electro-hydraulic actuator solution with open circuit architecture," Int. J. Fluid Power **22**(2), 233–258 (2021).

[36]J. D. Van de Ven, "On fluid compressibility in switch-mode hydraulic circuits—Part II: Experimental results," J. Dyn. Syst., Meas., Control **135**(2), 021014 (2013).
[37]V. H. Donkov, T. Andersen, M. Linjama, and M. Ebbesen, "Digital hydraulic technology for linear actuation: A state of the art review," Int. J. Fluid Power **21**(2), 263–304 (2020).
[38]J. J. Wu and J. D. Van de Ven, "Development of a high-speed on-off valve for switch-mode control of hydraulic circuits with four-quadrant control," in *Proceedings of the ASME 2010 International Mechanical Engineering Congress and Exposition* (ASME, Vancouver, BC, Canada, 2010), pp. 281–288.